Journal of Materials Chemistry A

ROYAL SOCIETY OF CHEMISTRY

PAPER

View Article Online
View Journal | View Issue

Check for updates

Cite this: J. Mater. Chem. A, 2024, 12, 31284

High performance all-polymer solar cells enabled with solvent and solid dual additives†

Misbah Sehar Abbasi,[a] Congqi Li,[a] Jinhua Gao,[a] Siying Wang,[a] Sixuan Wang,[a] Qijie Lin,[a] Gening Xie,[a] Saqib Nawaz Khan,[b] Jianqi Zhang,[c] Xin Zhang,[a] Yunhao Cai*[a] and Hui Huang*[a]

Morphology optimization of a photoactive layer has a crucial role in fabricating high-performance polymer solar cells (PSCs). If an active layer is cast from solution, then the unique properties of the donor and acceptor materials often lead to either excessive or insufficient phase separation, which adversely affect the performance of the device. Specifically, all-polymer solar cells (all-PSCs) introduce an added complexity in terms of morphology regulation due to the inherently flexible and entangled nature of polymer chains. In this work, we first introduced 3,5-dichloroanisole (DCA) as a solid additive, known for its good crystallinity and volatility, to refine the active-layer morphology in all-PSCs. Then, we combined 1-chloronaphthalene (CN) and DCA as dual additives, which effectively optimized the morphology of all-polymer blends. This combination favored charge transport and minimized charge recombination, leading to a higher fill factor across various systems. Notably, a device based on PM6:PY-DT processed with this dual-additives approach achieved an impressive power conversion efficiency (PCE) of 17.42%, outperforming the control device without any additive, which showed a PCE of 14.34%. Besides, dual additives were applied in other systems, revealing their universality. This work not only took advantages of both solvent and solid additives, but also effectively improved the performance of all-PSCs.

Received 25th August 2024
Accepted 9th October 2024

DOI: 10.1039/d4ta06013j

rsc.li/materials-a

1 Introduction

Polymer solar cells (PSCs) have emerged as a promising energy-harvesting technology for green energy thanks to their solution processability, lightweight, and flexibility.[1–6] The efficiency of small molecule-based PSCs has significantly increased recently owing to the swift progress in small-molecule acceptors (SMAs), illustrating their great potential of commercialization.[7–21] In general, all-PSCs are considered more suitable for practical use due to their excellent stretchability, mechanical robustness, and photo-thermal stability.[22–28] However, all-PSCs have received less attention and their power-conversion efficiencies (PCEs) are comparatively lower than those of their SMA-based counterparts.[29–36] One fundamental reason for their inferior performance lies in the difficulty in morphological control.[37–39] The unique characteristics of polymer donor and acceptor materials, as well as the large molecular size of polymers, increase the difficulty of controlling morphology.[40,41] In addition, the slow diffusion of polymer components during active-layer formation also leads to inadequate or excessive phase separation.[42] Consequently, effective methods for morphological control are needed urgently to adjust the phase separation for improving the performance of all-PSCs.

Many efforts have been devoted to optimize the morphology of PSCs, such as solvent vapor annealing, thermal annealing, solvent additive treatment and hot solution casting. Among them, use of a solvent additive is a widely adopted strategy of "tuning" the film morphology.[43–48] The morphology of PSCs can be manipulated closely by adding a tiny amount of the appropriate additive into the host system.[49–52] The influence of solvent additives on morphological control is associated with two characteristics: limited solvency to either donor or acceptor and low volatility.[53] This phenomenon indicates that solvent additives have a less volatile nature (due to a high boiling point) than the host solvent. This feature can lead to effective manipulation of aggregation of both the donor and acceptor and, hence, aid the formation of the desired phase separation during film formation. Besides solvent additives, solid additives with high crystallinity have attracted intense interest because they also show a favorable effect on controlling the self-assembly and phase separation of photovoltaic materials *via*

[a]College of Materials Science and Opto-Electronic Technology Center of Materials Science and Optoelectronics Engineering CAS Center for Excellence in Topological Quantum Computation CAS Key Laboratory of Vacuum Physics, University of Chinese Academy of Sciences, Beijing 100049, China. E-mail: caiyunhao@ucas.ac.cn; huihuang@ucas.ac.cn

[b]Institute of Physics, Chinese Academy of Sciences, Beijing 100190, China

[c]CAS Key Laboratory of Nanosystem and Hierarchical Fabrication, CAS Center for Excellence in Nanoscience, National Center for Nanoscience and Technology, Beijing 100190, China

† Electronic supplementary information (ESI) available. See DOI: https://doi.org/10.1039/d4ta06013j

various intermolecular interactions.[43,53–58] It has been shown that both solvent and solid additives can improve the performance of solar cells. Therefore, the combination of two types of additive is considered to be a simple (yet effective) approach to optimizing the morphology of the active layer. Nevertheless, morphological optimization involving two additives simultaneously and its impact on the photovoltaic performance of PSCs has seldom been investigated.[53,57,59–61]

Here, we developed a new strategy of tuning the morphology of all-polymer systems by incorporating the synergistic effects of solvent additive and volatilizable solid additive to achieve high-performance PSCs. Upon the use of the dual additives (CN + DCA), PM6:PY-DT based all-PSC realized a PCE of 17.42%, outperforming the devices processed with CN (16.42%) or DCA (16.57%). Systematic characterizations revealed that the enhanced efficiency could be attributed to the optimized morphology, facilitated charge transport and suppressed charge recombination. In addition, the developed dual additives (CN + DCA) were also applied successfully into PM6:PY-IT and PM6:PYF-T-o-based PSCs, demonstrating the universality of our strategy.

2 Results and discussion

Fig. 1a exhibits the molecular structures of PM6, PY-DT, CN and DCA. CN and DCA were selected as the solvent and solid additive, respectively. The energy levels of PM6 and PY-DT were estimated by cyclic voltammetry (Fig. 1c). The normalized UV-vis absorption spectra of the pristine films of PM6, PY-DT, DCA and the blend films are shown in Fig. 1d, e and S1,† respectively. It was found that, upon the use of dual additives, the absorption coefficient was obviously increased, which may benefit the J_{sc} of the corresponding device. To study the volatility of solid additive DCA, thermogravimetry analysis (TGA) was carried out first. TGA demonstrated that DCA underwent a gradual and continuous weight loss starting from 33 °C and reaching zero at ~90 °C (shown in Fig. S2†), suggesting the material was totally volatilized. This result indicated that DCA could be completely removed from the blend films after the thermal annealing (TA) procedure.

To study the effect of CN + DCA dual additives on the photovoltaic performance of PSCs, a series of devices with a conventional architecture of ITO/PEDOT:PSS/active layer/PNDIT:F3N/Ag were fabricated (Fig. 1b). Fig. 2a illustrates the current density–voltage (J–V) curves of optimized PM6:PY-DT-based PSCs under standard illumination (AM 1.5G) with 100 mW cm^{-2}. The photovoltaic parameters, including V_{oc}, J_{sc}, FF and PCE, are summarized in Tables 1 and S1.† PM6:PY-DT-based devices without any additive (device-I) achieved a PCE of 14.34% with a V_{oc} of 0.970 V, a J_{sc} of 23.86 mA cm^{-2} and an FF of 62.03%. The PM6:PY-DT device processed with a solvent additive of CN (device-II) showed a PCE of 16.42% with a V_{oc} of 0.962 V, a J_{sc} of 23.96 mA cm^{-2} and an FF of 71.20%. PM6:PY-DT-based devices with DCA as a solid additive (device-III) afforded a higher PCE of 16.57% with a V_{oc} of 0.974 V, a J_{sc} of 24.48 mA cm^{-2} and an FF of 69.44%. Impressively, PM6:PY-DT-based devices with dual additives (device-IV) secured an enhanced PCE of 17.42% with V_{oc}, J_{sc} and FF reaching up to 0.977 V, 24.57 mA cm^{-2} and 72.60%, respectively. The J_{sc} values were validated further by the external quantum efficiency (EQE) measurement, as demonstrated in Fig. 2b. Overall, all of the devices showed a high and broad EQE response in the

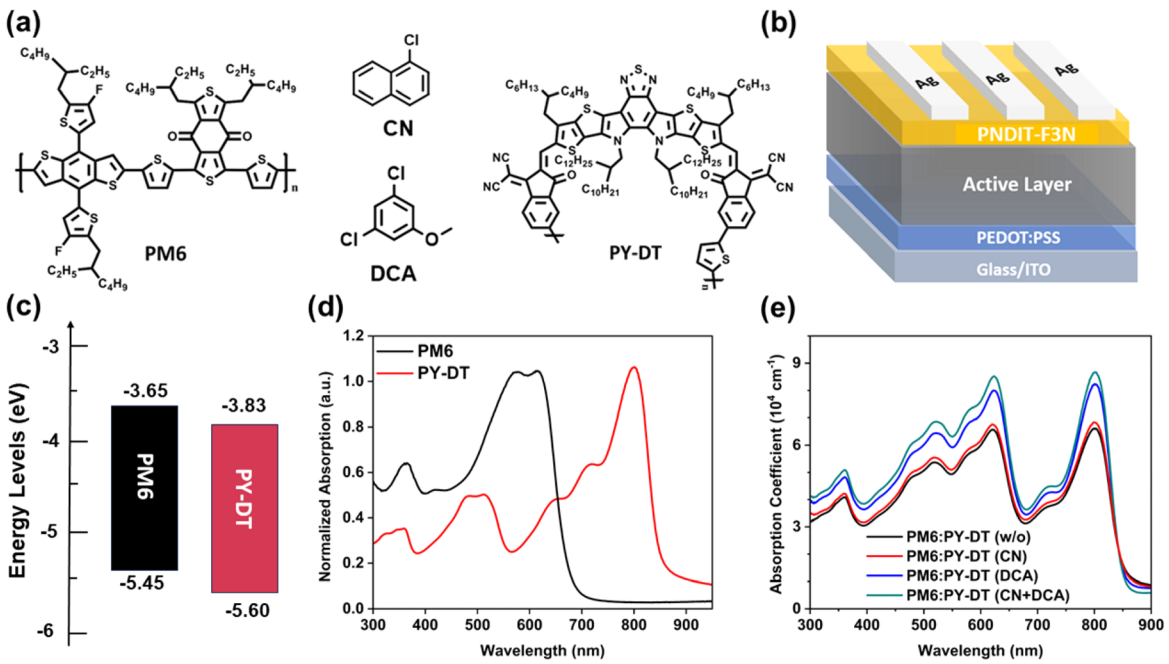

Fig. 1 (a) Chemical structures of PM6, PY-DT, CN and DCA. (b) Conventional device structure of PSCs. (c) Energy levels of PM6 and PY-DT. (d) Normalized absorption spectra of pristine films. (e) UV-vis absorption spectra of PM6:PY-DT blend films with different additive treatments.

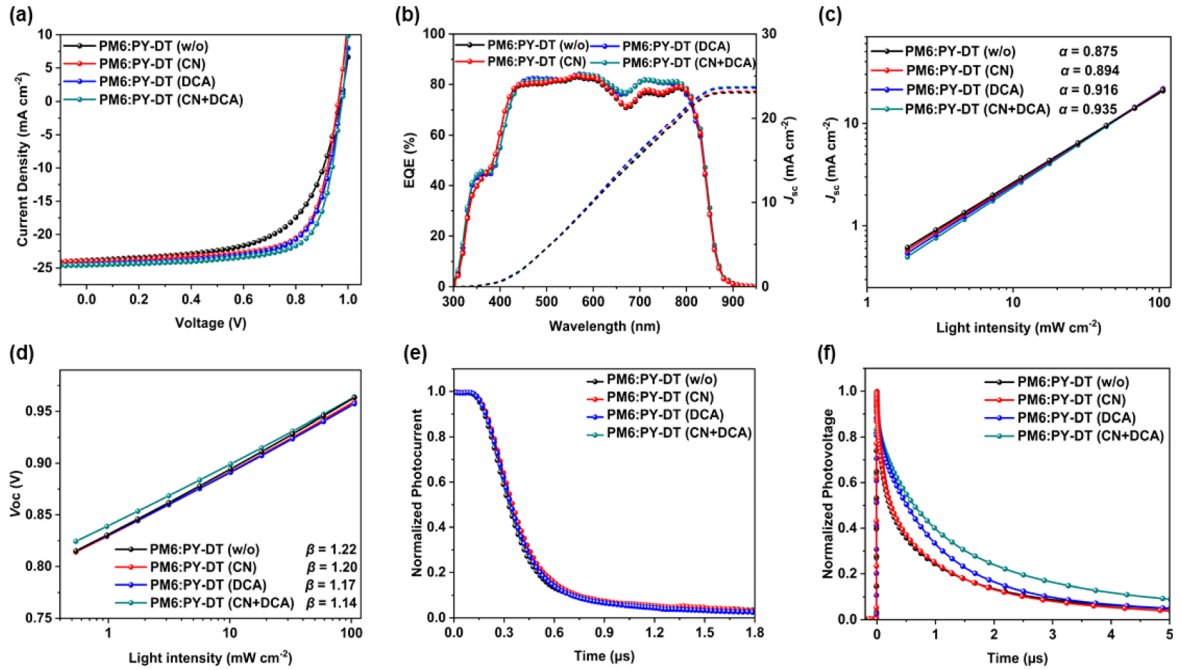

Fig. 2 (a) J–V characteristics and (b) EQE spectra and integrated J_{sc} of PM6:PY-DT fabricated under various conditions. (c) J_{sc} *vs.* light intensity and (d) V_{oc} *vs.* light intensity. (e) TPC and (f) TPV of PM6:PY-DT fabricated under various conditions.

wavelength range of 300–900 nm. Specifically, devices I, II, III and IV exhibited an integrated current density (J_{cal}) of 23.06, 23.18, 23.58 and 23.71 mA cm^{-2}, respectively, which were in good agreement with the values obtained from J–V measurements.

To study the influence of dual additives on the kinetics of charge recombination in PM6:PY-DT-based devices, both the J_{sc} and V_{oc} were plotted with respect to light intensity (P_{light}), as shown in Fig. 2c and d, respectively. The relationship between P_{light} and J_{sc} can be expressed as $J_{sc} \propto P_{light}^{\alpha}$, in which α is the slope of the curve. If the α is close to 1, then bimolecular recombination is suppressed under the short-circuit condition. The α values for devices I, II and III were determined to be 0.875, 0.894 and 0.916, respectively, while that of device IV exhibited a higher value of 0.935, which suggests a reduced bimolecular recombination in device IV, and thus contributed to the higher FF. The charge recombination kinetics of the devices were then explored by measuring the dependence of V_{oc} on the P_{light}. If the slope of V_{oc} *versus* the natural logarithm of P_{light} equals $\beta kT/q$, then bimolecular recombination has a major role within the device, where k is the Boltzmann constant, T is the temperature in Kelvin and q is the elementary charge. If trap-assisted recombination is involved, then a strong dependency of V_{oc} on the light intensity ($>kT/q$) will be obtained. The β vlaues for devices I, II, III and IV were 1.22, 1.20, 1.17, and 1.14, respectively, which showed that trap-assisted recombination had been suppressed by the dual additives.

The effect of dual additives on the carrier lifespan and charge extraction time of the PM6:PY-DT devices were evaluated by transient photovoltage (TPV) and transient photocurrent (TPC) measurements. Fig. 2e presents the TPC curves of PM6:PY-DT devices with treatment of different additives under various light intensities. The charge extraction time derived by fitting the TPC curves for devices I, II and III was 0.31, 0.22, and 0.20 μs, respectively, larger than that of device-IV (0.18 μs). Therefore, it can be inferred that the dual additives favored charge extraction in comparison with that of the other systems. The TPV curves of devices I–IV under various light intensities are exhibited in Fig. 2f. The carrier lifetime of devices I, II and III was determined to be 0.66, 0.72, and 1.02 μs, respectively, shorter than that of device-IV (1.25 μs). This observation

Table 1 Photovoltaic parameters of PM6:PY-DT-based devices fabricated with different additives

Additive	V_{oc} (V)	J_{sc} (mA cm^{-2})	FF (%)	PCE[a] (%)
w/o	0.970 (0.970 ± 0.02)	23.86 (23.85 ± 0.10)	62.03 (61.90 ± 0.55)	14.34 (14.31 ± 0.27)
CN	0.962 (0.968 ± 0.05)	23.96 (23.90 ± 0.12)	71.20 (71.15 ± 0.72)	16.42 (16.34 ± 0.25)
DCA	0.974 (0.970 ± 0.04)	24.48 (24.42 ± 0.25)	69.44 (69.10 ± 0.63)	16.57 (16.35 ± 0.29)
CN + DCA	0.977 (0.974 ± 0.003)	24.57 (24.50 ± 0.15)	72.60 (71.87 ± 0.30)	17.42 (17.36 ± 0.10)

[a] The numerical values in brackets were obtained from the statistical data of 10 independent devices.

suggested that dual-additives could be effective in increasing the charge mobility and reducing the charge recombination.

To investigate the effect of dual additives on charge generation and dissociation processes, a graph between photocurrent density (J_{ph}) and effective voltage (V_{eff}) was plotted (Fig. S3†). J_{ph} is defined as $J_{ph} = J_L - J_D$, and V_{eff} is denoted as $V_{eff} = V_0 - V_a$, in which V_0 is the voltage at which J_{ph} is zero, and V_a is the applied bias voltage. When the J_{ph} reached saturation at V_{eff} of 2 V, the saturation value (J_{sat}) of devices I, II, III and IV was 25.17, 24.94, 25.21, and 25.26 mA cm^{-2}, respectively. The exciton dissociation probability $P(E,T)$ was assessed by normalizing J_{ph} with respect to J_{sat} (J_{ph}/J_{sat}) under the short-circuit condition. The $P(E,T)$ values of devices I, II, III and IV were 94.7%, 96%, 97% and 97.2%, respectively. These observations revealed that the dual-additives were beneficial for charge generation and dissociation processes. The space-charge limited current (SCLC) method was carried out to explore the charge mobilities of devices I–IV. Devices with configurations of ITO/PEDOT:PSS/active layer/MoO_3/Ag and ITO/ZnO/active layer/PNDIT-F3N/Ag were fabricated to obtain the hole and electron mobilities, respectively. Fig. S4† illustrates the plots of $J^{1/2}$–V for electron-only and hole-only devices, and Table S2† summarizes the corresponding electron (μ_e) and hole (μ_h) mobilities. Among devices I–IV, device IV processed with dual additives exhibited the highest μ_e and μ_h of 3.40×10^{-4} and 3.19×10^{-4} cm^2 V^{-1} s^{-1}, respectively. Besides, the ratio of the hole/electron mobility μ_h/μ_e was 1.50, 1.29, 1.25, and 1.06 for devices I, II, III and IV, respectively. The highest mobility and most balanced charge transport properties of device IV processed with dual additives may have contributed to the highest J_{sc} and FF.

To investigate the miscibility of DCA between PM6 and PY-DT by the Flory–Huggins interaction parameter (χ), contact-angle measurements were performed, as illustrated in Fig. S5.† The surface free energy (γ) of PM6, PY-DT and DCA calculated by Wu's model was 25.76, 26.60 and 28.96 mN m^{-1}, respectively (Table S3†). The Flory–Huggins interaction parameters of PM6/DCA, PY-DT/PM6, and PY-DT/DCA were calculated to be 1.79, 1.1 and 0.16, respectively, which suggested that DCA had higher miscibility with PY-DT in contrast to PM6. Due to the favorable miscibility of DCA and PY-DT, DCA can restrain the over self-assembly of PY-DT amidst the film-casting process, leading to a conducive PM6 and PY-DT matrix after DCA elimination during TA treatment.

Atomic force microscopy (AFM) was employed to examine the surface morphology of PM6:PY-DT blend films subjected to various processing conditions, as shown in Fig. 3(a–d) and S6(a–d).† Obviously, the PM6:PY-DT blend film of device I exhibited a smooth surface with large crystalline bulk and root mean square (RMS) of 1.00 nm. The blend processed with CN revealed an RMS of 0.90 nm, while the blend using DCA as the solid additive presented an RMS of 1.15 nm. In particular, the dual additives-treated blend (device IV) showed improved crystallization, which helped polymer growth with an RMS of 1.49 nm. Fig. S7† exhibits the TEM images of the blends. The blend film treated by dual additives showed a more obvious fibrillar morphology. This is beneficial to efficient exciton dissociation and charge transport.

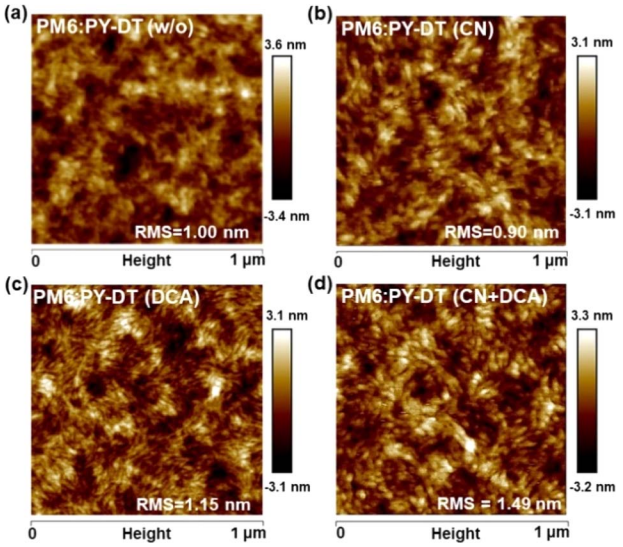

Fig. 3 (a–d) AFM height images of PM6:PY-DT blend films fabricated under various conditions.

To examine the molecular packing and crystallinities of PM6:PY-DT blend films, grazing-incidence wide angle X-ray scattering (GIWAXS) analyses were conducted. Fig. 4 displays both the two-dimensional (2D) GIWAXS patterns and their respective line cuts, and a comprehensive summary of diffraction peaks are provided in Tables S4 and S5,† respectively. PM6:PY-DT (w/o) film exhibited clear π–π stacking (010) peaks at $q_z = 1.650$ (d-spacing = 3.80 Å) along the out-of-plane (OOP) direction and lamellar stacking (100) peaks at $q_{xy} = 0.304$ (d-spacing = 20.65 Å) along the in-plane (IP) direction, suggesting that molecular packing was preferably face on-oriented with regard to the substrate. Upon adding CN or DCA additives in PM6:PY-DT blends, CCL values related to both the lamellar (100) and π–π stacking (010) peaks increased, which suggested that CN and DCA could both improve the crystallinity and molecular order of the PM6:PY-DT blend. PM6:PY-DT blend films with dual-additive treatment exhibited a stronger π–π stacking (010) peak and a higher CCL from 17.00 to 22.15 Å. Furthermore, a similar trend was observed along lamellar stacking, where CCL values increased from 102.16 to 107.27 Å. Hence, the blend film with dual additives had a more ordered crystalline structure. With the synergistic effect of CN and DCA, molecular packing was effectually adjusted, which is advantageous for achieving higher charge carrier mobility and FF in the corresponding devices.

To investigate the generality of the dual additives, we further applied the strategy to PM6:PY-IT and PM6:PYF-T-o systems (Fig. S8†). Fig. S9a and S10a† show the J–V curves of the corresponding devices with different treatments. Tables S6 and S7† summarize the photovoltaic parameters of the corresponding devices. PM6:PY-IT without any additive achieved a PCE of 15.27%. Impressively, PM6:PY-IT-based devices with the dual additives of CN + DCA secured a remarkable PCE of 16.76%. The PM6:PYF-T-o-based PSCs processed without an additive showed a PCE of 12.24%. As expected, treatment with dual additives

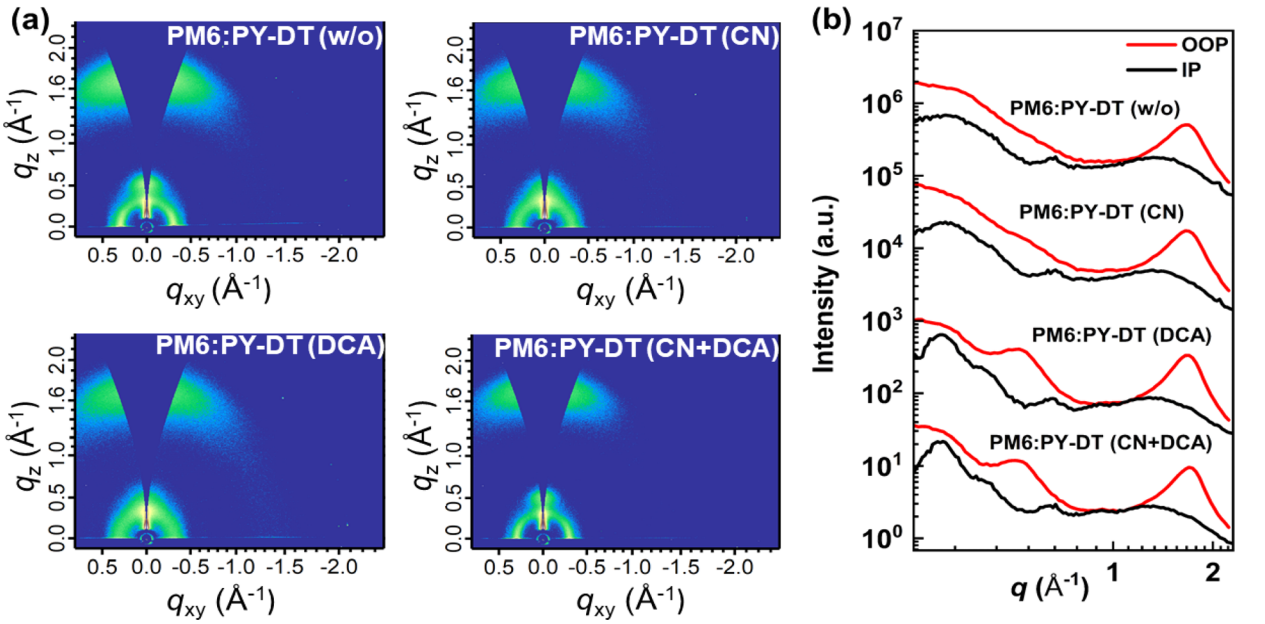

Fig. 4 (a) 2D GIWAXS scattering patterns of PM6:PY-DT blends fabricated under various conditions. (b) Line-cut profiles in IP and OOP directions from GIWAXS images of PM6:PY-DT blends fabricated under various conditions.

markedly increased the PCE to 16.37%. The improved J_{sc} was further confirmed by the EQE test. It is worth mentioning that the synergistic effect of the CN and DCA resulted in significantly enhanced FF values and higher PCEs of the corresponding PSCs.

To address the stability requirements for practical applications, we further investigated the storage stability of unencapsulated devices. PM6:PY-DT-based devices processed under different conditions were stored in a N_2-filled glove box. The times required to reach 80% of the initial performance (T_{80}) of all-PSCs processed with CN, DCA and CN + DCA were 473, 794 and 670 h, respectively, as shown in Fig. S11.† These data highlighted the importance of additive selection for enhancing the long-term stability of all-PSCs. These findings convincingly demonstrate that the introduction of dual additives synergistically enhances both device performance and stability.

3 Conclusion

We developed a novel dual-additives strategy to regulate the morphology of all-polymer blends, in which a solid additive DCA was combined with CN to synergistically optimize molecular organization and phase separation. These improvements helped to enhance charge transport and extraction efficiency while reducing charge recombination. Consequently, the PM6:PY-DT-based OSCs treated with dual additives achieved a PCE of 17.42%, much higher than that of the devices without any additive (14.34%). Moreover, this approach was successfully extended to other material systems, thereby manifesting its universality. This work provides a new idea of regulating bulk heterojunction morphology towards the development of highly efficient all-PSCs.

Data availability

The data that support the findings of this study are available in the ESI.†

Conflicts of interest

The authors declare no conflict of interest.

Acknowledgements

The authors acknowledge financial support from the NSFC (52103352, 51925306, and 52120105006), National Key R&D Program of China (2018FYA0305800), Key Research Program of the Chinese Academy of Sciences (XDPB08-2, E3E41805X2), the Strategic Priority Research Program of the Chinese Academy of Sciences (XDB28000000), the Youth Innovation Promotion Association of the Chinese Academy of Sciences (2022165), and the Fundamental Research Funds for the Central Universities. One author was sponsored by the ANSO scholarship for young talent.

References

1 G. Yu, J. Gao, J. C. Hummelen, F. Wudl and A. J. Heeger, *Science*, 1995, **270**, 1789–1791.
2 A. Khasbaatar, Z. Xu, J.-H. Lee, G. Campillo-Alvarado, C. Hwang, B. N. Onusaitis and Y. Diao, *Chem. Rev.*, 2023, **123**, 8395–8487.
3 B. Liu, R.-Q. Png, L.-H. Zhao, L.-L. Chua, R. H. Friend and P. K. H. Ho, *Nat. Commun.*, 2012, **3**, 1321.
4 K. Weng, L. Ye, L. Zhu, J. Xu, J. Zhou, X. Feng, G. Lu, S. Tan, F. Liu and Y. Sun, *Nat. Commun.*, 2020, **11**, 2855.

5 D. Baran, R. S. Ashraf, D. A. Hanifi, M. Abdelsamie, N. Gasparini, J. A. Röhr, S. Holliday, A. Wadsworth, S. Lockett, M. Neophytou, C. J. M. Emmott, J. Nelson, C. J. Brabec, A. Amassian, A. Salleo, T. Kirchartz, J. R. Durrant and I. McCulloch, *Nat. Mater.*, 2017, **16**, 363–369.
6 H. Kang, G. Kim, J. Kim, S. Kwon, H. Kim and K. Lee, *Adv. Mater.*, 2016, **28**, 7821–7861.
7 H. Li, B. Yu and H. Yu, *Adv. Funct. Mater.*, 2024, **34**, 2402128.
8 S. Shen, Y. Mi, Y. Ouyang, Y. Lin, J. Deng, W. Zhang, J. Zhang, Z. Ma, C. Zhang, J. Song and Z. Bo, *Angew. Chem., Int. Ed.*, 2023, **62**, e202316495.
9 J. Fu, Q. Yang, P. Huang, S. Chung, K. Cho, Z. Kan, H. Liu, X. Lu, Y. Lang, H. Lai, F. He, P. W. K. Fong, S. Lu, Y. Yang, Z. Xiao and G. Li, *Nat. Commun.*, 2024, **15**, 1830.
10 L. Tian, C. Liu and F. Huang, *Sci. China: Chem.*, 2024, **67**, 788–805.
11 Z. Li, K. Jiang, G. Yang, J. Y. L. Lai, T. Ma, J. Zhao, W. Ma and H. Yan, *Nat. Commun.*, 2016, **7**, 13094.
12 Y. Wei, Z. Chen, G. Lu, N. Yu, C. Li, J. Gao, X. Gu, X. Hao, G. Lu, Z. Tang, J. Zhang, Z. Wei, X. Zhang and H. Huang, *Adv. Mater.*, 2022, **34**, 2204718.
13 J. Gao, N. Yu, Z. Chen, Y. Wei, C. Li, T. Liu, X. Gu, J. Zhang, Z. Wei, Z. Tang, X. Hao, F. Zhang, X. Zhang and H. Huang, *Adv. Sci.*, 2022, **9**, 2203606.
14 H. Chen, W. Sun, R. Zhang, Y. Huang, B. Zhang, G. Zeng, J. Ding, W. Chen, F. Gao, Y. Li and Y. Li, *Adv. Mater.*, 2024, **36**, 2402350.
15 X. Xu, W. Jing, H. Meng, Y. Guo, L. Yu, R. Li and Q. Peng, *Adv. Mater.*, 2023, **35**, 2208997.
16 C. Guo, Y. Sun, L. Wang, C. Liu, C. Chen, J. Cheng, W. Xia, Z. Gan, J. Zhou, Z. Chen, J. Zhou, D. Liu, J. Guo, W. Li and T. Wang, *Energy Environ. Sci.*, 2024, **17**, 2492–2499.
17 Z. Fu, J. Qiao, F. Cui, W. Zhang, L. Wang, P. Lu, H. Yin, X. Du, W. Qin and X. Hao, *Adv. Mater.*, 2024, **36**, 2313532.
18 D. Qiu, C. Tian, H. Zhang, J. Zhang, Z. Wei and K. Lu, *Adv. Mater.*, 2024, **36**, 2313251.
19 J. Song and Z. Bo, *Chin. Chem. Lett.*, 2023, **34**, 108163.
20 J. Tan, Y. Zhao, G. Li, S. Yang, C. Huang and H. Yu, *Adv. Funct. Mater.*, 2022, **32**, 2209094.
21 Q. Yang, R. Wu, L. Yang, W. Liu, X. Meng, W. Zhang, S. Shen, M. Li, Y. Zhou and J. Song, *Dyes Pigm.*, 2024, **221**, 111808.
22 E. Zhou, J. Cong, Q. Wei, K. Tajima, C. Yang and K. Hashimoto, *Angew. Chem., Int. Ed.*, 2011, **50**, 2799–2803.
23 T. Kim, J.-H. Kim, T. E. Kang, C. Lee, H. Kang, M. Shin, C. Wang, B. Ma, U. Jeong, T.-S. Kim and B. J. Kim, *Nat. Commun.*, 2015, **6**, 8547.
24 H. Yu, M. Pan, R. Sun, I. Agunawela, J. Zhang, Y. Li, Z. Qi, H. Han, X. Zou, W. Zhou, S. Chen, J. Y. L. Lai, S. Luo, Z. Luo, D. Zhao, X. Lu, H. Ade, F. Huang, J. Min and H. Yan, *Angew. Chem., Int. Ed.*, 2021, **60**, 10137–10146.
25 H. Fu, Y. Li, J. Yu, Z. Wu, Q. Fan, F. Lin, H. Y. Woo, F. Gao, Z. Zhu and A. K.-Y. Jen, *J. Am. Chem. Soc.*, 2021, **143**, 2665–2670.
26 T. Liu, T. Yang, R. Ma, L. Zhan, Z. Luo, G. Zhang, Y. Li, K. Gao, Y. Xiao, J. Yu, X. Zou, H. Sun, M. Zhang, T. A. Dela Peña, Z. Xing, H. Liu, X. Li, G. Li, J. Huang, C. Duan, K. S. Wong, X. Lu, X. Guo, F. Gao, H. Chen, F. Huang, Y. Li, Y. Li, Y. Cao, B. Tang and H. Yan, *Joule*, 2021, **5**, 914–930.
27 J. Du, K. Hu, J. Zhang, L. Meng, J. Yue, I. Angunawela, H. Yan, S. Qin, X. Kong, Z. Zhang, B. Guan, H. Ade and Y. Li, *Nat. Commun.*, 2021, **12**, 5264.
28 R. Sun, W. Wang, H. Yu, Z. Chen, X. Xia, H. Shen, J. Guo, M. Shi, Y. Zheng, Y. Wu, W. Yang, T. Wang, Q. Wu, Y. (Michael) Yang, X. Lu, J. Xia, C. J. Brabec, H. Yan, Y. Li and J. Min, *Joule*, 2021, **5**, 1548–1565.
29 Y. Cai, C. Xie, Q. Li, C. Liu, J. Gao, M. H. Jee, J. Qiao, Y. Li, J. Song, X. Hao, H. Y. Woo, Z. Tang, Y. Zhou, C. Zhang, H. Huang and Y. Sun, *Adv. Mater.*, 2023, **35**, 2208165.
30 B. Li, X. Zhang, Z. Wu, J. Yang, B. Liu, Q. Liao, J. Wang, K. Feng, R. Chen, H. Y. Woo, F. Ye, L. Niu, X. Guo and H. Sun, *Sci. China: Chem.*, 2022, **65**, 1157–1163.
31 Z. Luo, T. Liu, R. Ma, Y. Xiao, L. Zhan, G. Zhang, H. Sun, F. Ni, G. Chai, J. Wang, C. Zhong, Y. Zou, X. Guo, X. Lu, H. Chen, H. Yan and C. Yang, *Adv. Mater.*, 2020, **32**, 2005942.
32 H. Sun, H. Yu, Y. Shi, J. Yu, Z. Peng, X. Zhang, B. Liu, J. Wang, R. Singh, J. Lee, Y. Li, Z. Wei, Q. Liao, Z. Kan, L. Ye, H. Yan, F. Gao and X. Guo, *Adv. Mater.*, 2020, **32**, 2004183.
33 J. Du, K. Hu, L. Meng, I. Angunawela, J. Zhang, S. Qin, A. Liebman-Pelaez, C. Zhu, Z. Zhang, H. Ade and Y. Li, *Angew. Chem., Int. Ed.*, 2020, **59**, 15181–15185.
34 Y. Wu, S. Schneider, C. Walter, A. H. Chowdhury, B. Bahrami, H.-C. Wu, Q. Qiao, M. F. Toney and Z. Bao, *J. Am. Chem. Soc.*, 2020, **142**, 392–406.
35 H. Yu, Z. Qi, J. Yu, Y. Xiao, R. Sun, Z. Luo, A. M. H. Cheung, J. Zhang, H. Sun, W. Zhou, S. Chen, X. Guo, X. Lu, F. Gao, J. Min and H. Yan, *Adv. Energy Mater.*, 2021, **11**, 2003171.
36 W. Wang, Q. Wu, R. Sun, J. Guo, Y. Wu, M. Shi, W. Yang, H. Li and J. Min, *Joule*, 2020, **4**, 1070–1086.
37 Z. Li, W. Zhong, L. Ying, F. Liu, N. Li, F. Huang and Y. Cao, *Nano Energy*, 2019, **64**, 103931.
38 H. Benten, D. Mori, H. Ohkita and S. Ito, *J. Mater. Chem. A*, 2016, **4**, 5340–5365.
39 X. Liu, C. Zhang, C. Duan, M. Li, Z. Hu, J. Wang, F. Liu, N. Li, C. J. Brabec, R. A. J. Janssen, G. C. Bazan, F. Huang and Y. Cao, *J. Am. Chem. Soc.*, 2018, **140**, 8934–8943.
40 Y. Zhang, B. Wu, Y. He, W. Deng, J. Li, J. Li, N. Qiao, Y. Xing, X. Yuan, N. Li, C. J. Brabec, H. Wu, G. Lu, C. Duan, F. Huang and Y. Cao, *Nano Energy*, 2022, **93**, 106858.
41 N. Wang, X. Long, Z. Ding, J. Feng, B. Lin, W. Ma, C. Dou, J. Liu and L. Wang, *Macromolecules*, 2019, **52**, 2402–2410.
42 G. Wang, F. S. Melkonyan, A. Facchetti and T. J. Marks, *Angew. Chem., Int. Ed.*, 2019, **58**, 4129–4142.
43 L. Zhu, W. Zhong, C. Qiu, B. Lyu, Z. Zhou, M. Zhang, J. Song, J. Xu, J. Wang, J. Ali, W. Feng, Z. Shi, X. Gu, L. Ying, Y. Zhang and F. Liu, *Adv. Mater.*, 2019, **31**, 1902899.
44 B. Liu, H. Sun, J.-W. Lee, J. Yang, J. Wang, Y. Li, B. Li, M. Xu, Q. Liao, W. Zhang, D. Han, L. Niu, H. Meng, B. J. Kim and X. Guo, *Energy Environ. Sci.*, 2021, **14**, 4499–4507.
45 Q. Wu, W. Wang, T. Wang, R. Sun, J. Guo, Y. Wu, X. Jiao, C. J. Brabec, Y. Li and J. Min, *Sci. China: Chem.*, 2020, **63**, 1449–1460.

46 M. Xiao, L. Liu, Y. Meng, B. Fan, W. Su, C. Jin, L. Liao, F. Yi, C. Xu, R. Zhang, A. K.-Y. Jen, W. Ma and Q. Fan, *Sci. China: Chem.*, 2023, **66**, 1500–1510.
47 Y. Su, Z. Ding, R. Zhang, W. Tang, W. Huang, Z. Wang, K. Zhao, X. Wang, S. Liu and Y. Li, *Sci. China: Chem.*, 2023, **66**, 2380–2388.
48 Y. Liu, B. Liu, C.-Q. Ma, F. Huang, G. Feng, H. Chen, J. Hou, L. Yan, Q. Wei, Q. Luo, Q. Bao, W. Ma, W. Liu, W. Li, X. Wan, X. Hu, Y. Han, Y. Li, Y. Zhou, Y. Zou, Y. Chen, Y. Liu, L. Meng, Y. Li, Y. Chen, Z. Tang, Z. Hu, Z.-G. Zhang and Z. Bo, *Sci. China: Chem.*, 2022, **65**, 1457–1497.
49 Y. Yao, J. Hou, Z. Xu, G. Li and Y. Yang, *Adv. Funct. Mater.*, 2008, **18**, 1783–1789.
50 F. Zhao, C. Wang and X. Zhan, *Adv. Energy Mater.*, 2018, **28**, 1703147.
51 H.-C. Liao, C.-C. Ho, C.-Y. Chang, M.-H. Jao, S. B. Darling and W.-F. Su, *Mater. Today*, 2013, **16**, 326–336.
52 M. A. Brady, G. M. Su and M. L. Chabinyc, *Soft Matter*, 2011, **7**, 11065.
53 S. Bao, H. Yang, H. Fan, J. Zhang, Z. Wei, C. Cui and Y. Li, *Adv. Mater.*, 2021, **33**, 2105301.
54 C. Li, X. Gu, Z. Chen, X. Han, N. Yu, Y. Wei, J. Gao, H. Chen, M. Zhang, A. Wang, J. Zhang, Z. Wei, Q. Peng, Z. Tang, X. Hao, X. Zhang and H. Huang, *J. Am. Chem. Soc.*, 2022, **144**, 14731–14739.
55 K. Hu, C. Zhu, K. Ding, S. Qin, W. Lai, J. Du, J. Zhang, Z. Wei, X. Li, Z. Zhang, L. Meng, H. Ade and Y. Li, *Energy Environ. Sci.*, 2022, **15**, 4157–4166.
56 J. Fu, P. W. K. Fong, H. Liu, C.-S. Huang, X. Lu, S. Lu, M. Abdelsamie, T. Kodalle, C. M. Sutter-Fella, Y. Yang and G. Li, *Nat. Commun.*, 2023, **14**, 1760.
57 C. Fan, H. Yang, Q. Zhang, S. Bao, H. Fan, X. Zhu, C. Cui and Y. Li, *Sci. China: Chem.*, 2021, **64**, 2017–2024.
58 J. Song, Y. Li, Y. Cai, R. Zhang, S. Wang, J. Xin, L. Han, D. Wei, W. Ma, F. Gao and Y. Sun, *Matter*, 2022, **5**, 4047–4059.
59 H. Liu, Y. Fu, Z. Chen, J. Wang, J. Fu, Y. Li, G. Cai, C. Su, U. Jeng, H. Zhu, G. Li and X. Lu, *Adv. Funct. Mater.*, 2023, **33**, 2303307.
60 R. Wang, M. Wu, D. Zhang, G. Yang, D. Zheng and J. Yu, *Synth. Met.*, 2024, **304**, 117586.
61 Y.-N. Yang, X.-M. Li, S.-J. Wang, X.-P. Duan, Y.-H. Cai, X.-B. Sun, D.-H. Wei, W. Ma and Y.-M. Sun, *Chin. J. Polym. Sci.*, 2023, **41**, 194–201.